Orthotropic material properties of the gerbil basilar membrane

Shuangqin Liu and Robert D. White[a)]
Mechanical Engineering Department, Tufts University, 200 College Avenue, Medford, Massachusetts 02155

(Received 2 July 2007; revised 15 January 2008; accepted 16 January 2008)

In this paper, two sets of experimental results to extract the two effective elastic moduli, the effective shear modulus, and the effective Poisson's ratio for the gerbil cochlear partition are analyzed. In order to accomplish this, a geometrically nonlinear composite orthotropic plate model is employed. The model is used to predict both out-of-plane and in-plane motion of the partition under a static finite area distributed load. This loading condition models the small, but finite size, probe tips used in experiments. Both in-plane and out-of-plane motion are needed for comparison with recent experimental results. It is shown that the spatial decay rate (the space constant) for the in-plane deflection is different than for the out-of-plane deflection, which has a significant effect on the derived partition properties. The size of the probe tip is shown to have little influence on the results. Results are presented for two types of boundary conditions. Orthotropy ratios determined from the experimental data are found to vary with longitudinal position and choice of boundary conditions. Orthotropy ratios (the ratio of the two elastic moduli) are in the range of 65 close to the base to 10 in the upper middle turn of the cochlea. © *2008 Acoustical Society of America.*
[DOI: 10.1121/1.2871682]

PACS number(s): 43.64.Bt, 43.64.Kc [BLM] Pages: 2160–2171

I. INTRODUCTION

The accuracy of mechanical models of traveling fluid-structure waves in the cochlea depend on accurate structural models for the cochlear partition. The cochlear partition has variously been modeled as a locally reacting impedance (Lynch *et al.*, 1982; Neely and Kim, 1986; Ramamoorthy *et al.*, 2007) a one dimensional beam (Allaire *et al.*, 1974; Miller, 1985), a two-dimensional orthotropic plate (Steele and Taber, 1979), or a two-dimensional orthotropic pretensioned plate (Naidu and Mountain, 2007). The parameters required for each of these models can be determined from a knowledge of the geometry and the pointwise effective material properties of the cochlear partition. Geometry can be determined from physiological studies (Schweitzer *et al.*, 1996; Edge *et al.*, 1998). Pointwise effective material properties must be determined indirectly by observing the response of the structure *in vivo* to carefully conducted experiments.

This paper focuses on determination of effective pointwise material properties using point load experiments published by Naidu and Mountain (1998; 2001) and Emadi *et al.* (2004). A particular aim of this work is to quantify the orthotropic properties of the cochlear partition. It is well known that the cochlear partition is orthotropic, based on physiology (Iurato, 1962; Miller, 1985), qualitative observations of static partition deflection (Voldrich, 1978), and quantitative dynamic measurements (Richter *et al.*, 1998). However, most prior quantitative static experimental work gave only point stiffness measurements (Gummer *et al.*, 1981; Miller, 1985; Olson and Mountain, 1991; Naidu and Mountain, 1998), from which it is not possible to determine orthotropic properties.

In 2001, quantitative measurements of the *shape* of the deflected region during point load experiments were made by Naidu and Mountain (2001). These experiments allow quantitative determination of the level of orthotropy. In Naidu and Mountain (2001), the BM was deflected from 1 to 15 μm in a 1 μm increment. In addition to the point stiffness, the shape of the *lateral* deflection region was measured quantitatively for each case. The normalized shape of the lateral deflection profile exhibited exponential decay away from the center; the exponent characterizing this decay was expressed as a "space constant." Two sets of space constants were reported in their paper. One was with the organ of Corti present and the other is with the organ of Corti removed. The space constant used in this paper was the one with the organ of Corti present. In Emadi *et al.* (2004), the point stiffness of the cochlear partition in a hemicochlea preparation was measured as a function of distance from the cut edge. The variation of stiffness as a function of distance from the cut edge is related to longitudinal coupling in the cochlear partition, albeit in a different way than the lateral deflection results of Naidu and Mountain.

In this paper, we use these two sets of experimental results to extract the two effective elastic moduli, the effective shear modulus, and the effective Poisson's ratio for the cochlear partition. In order to accomplish this, we employ a geometrically nonlinear composite orthotropic plate model. Despite the small deflections, a nonlinear geometric model must be used in order to determine *lateral deflections*, which are not present in a linear plate model. The *lateral deflections* are the quantities measured by Naidu and Mountain. We show that the shape of the lateral deflection is not the same as the shape of the vertical deflection; thus it is not correct to assume that the shape constant for the vertical deflection is the same as the shape constant for the lateral deflection.

[a)]Electronic mail: r.white@tufts.edu

 0001-4966/2008/123(4)/2160/12/$23.00

Two boundary conditions for the model were investigated. The first is all four edges of the plate simply supported (SS). The second is one edge clamped and others simply supported (CS). Based on the stiffness and space constant reported in Naidu and Mountain with the organ of Corti present, we determine the following: using SS boundary conditions, the radial elastic modulus decreases from 15 to 1 MPa from base to the upper middle turn of gerbil cochlea; longitudinal modulus decreases from 0.2 to 0.05 MPa. Using CS boundary conditions, radial elastic modulus decreases from 6.6 to 0.5 MPa from base to the upper middle turn of gerbil cochlea; longitudinal modulus decreases from 0.4 to 0.05 MPa. The orthotropy varies along the length of the cochlear partition from a maximum of 65 close to the base to a minimum of 10 in the upper middle turn. We also investigate the effect of changing probe contact area for the point measurements, showing that for probes of radius from 2 to 12.5 μm, the probe diameter has little effect on the shape of the deflected region.

The material properties computed based on the experimental data in Emadi *et al.*, which was measured approximately two-thirds of the way from base to apex, suggest considerably less orthotropy than Naidu and Mountain's data. Using the SS boundary condition, Emadi *et al.*'s data suggest a transverse modulus of 0.048 MPa and a longitudinal modulus of 0.026 MPa. Using the CS boundary condition, the transverse modulus is 0.025 MPa and the longitudinal modulus is 0.023 MPa.

The physiology of the cochlea partition is more complicated than the model we used. For instance, the stiffness measurements can easily be affected by factors including the organ of Corti (Naidu and Mountain, 1998), and the tectorial membrane (Emadi *et al.*, 2004). The stiffness is not uniform in arcuate zone or pectinate zone (Naidu and Mountain, 1998). Radial pretension may also be present (Naidu and Mountain, 2007). If all the complexities are embedded in the model, there would be too many free parameters to be determined. By simplifying the model, and thus reducing the number of the free parameters, we can use currently available experiment data to compute the effective material properties. Thus, pretension, radial variation and the tectorial membrane are not included in our current model, as they are not needed to explain the observed longitudinally varying space constants and point stiffness.

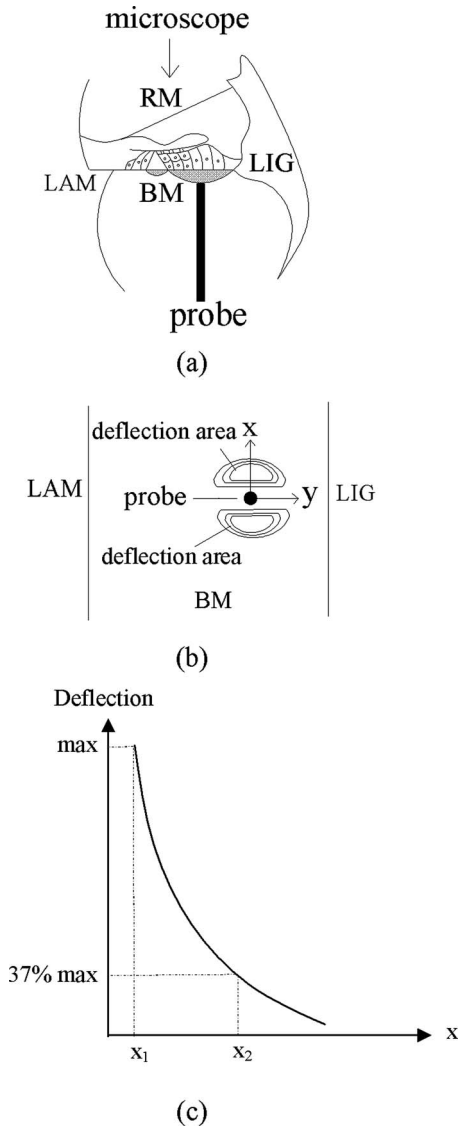

FIG. 1. Schematic of BM stiffness measurement procedure from Naidu and Mountain (1998, 2001): (a) A circular probe is pushed into the cochlear partition, and the force vs deflection curve is measured; (b) a top-down view of BM; the contours show the shape of the lateral (x direction) deflections (c) deflection space constant is described as the distance x_2-x_1 along the x direction where the deflection decreases exponentially from its maximum value to 37% of maximum value. In this drawing, BM is the basilar membrane, LAM is the spiral lamina, and LIG is the spiral ligament.

II. MATHEMATICAL MODEL

The structural model used herein is best understood by considering the experiments it is used to analyze, shown schematically in Fig. 1. This experimental work (Naidu and Mountain, 1998, 2001), provides two pieces of information: (1) point stiffness, which is measured by pushing a probe into the partition and reporting the deflection versus restoring force, and (2) the space constant, which is the distance from the location of the probe that the *lateral* deflection of a mark on the cochlear partition reduces to 37% of its maximum level.

We emphasize again that in the cited experimental work, the space constant was determined by observing *lateral* deflections of the cochlear partition using microscopy (Naidu and Mountain, 2001). A linear plate model has no lateral deflections. However, a geometrically nonlinear plate model (for deflection amplitudes as applied in the experiment) does experience observable lateral deflections. It was assumed by Naidu and Mountain that the out-of-plane deflections were proportional to these observed lateral deflections. The major motivation for the use of a geometrically nonlinear plate model in this work is to explore the validity of the assumed proportionality between out of plane and lateral deflections, and potential effects on predictions of the small-deflection material properties.

The orthotropic composite plate model used here requires four independent material properties: elastic moduli in both longitudinal and transverse directions (E_x, E_y), shear

modulus (G_{xy}), and Poisson's ratio (ν_{xy}). These properties must be determined to match the point stiffness and space constants that have been reported. Since there are four quantities to determine, but only two available measurements, some additional assumptions must be made based on composite plate theory. These are explained in detail in the following.

The overall procedure is as follows. First, an Euler–Bernoulli beam model with a single material property, E_y, is used to match point stiffness data (Naidu and Mountain, 1998; Emadi *et al.*, 2004). This gives an initial estimate of the transverse plate modulus, E_y. An orthotropy ratio, E_y/E_x, is then arbitrarily chosen. E_y/E_x is always in the range 1–1000. With E_y/E_x chosen, it is possible to compute G_{xy} and ν_{xy} by making use of a composite plate material model, as explained in the following. With all four plate constants in hand, a linear analytic plate model or a nonlinear finite element scheme is then used to compute the shape of the deflected region produced by a finite area static probe load. The point stiffness and space constant are determined from the result, and compared to that reported in the experimental data. The values of E_y and E_x are then adjusted, G_{xy} and ν_{xy} recomputed, and the procedure repeated until a match with experiment is obtained.

Two sets of boundary conditions have been employed by previous authors modeling the cochlear partition. In some works, one edge is taken to be simply supported and the other clamped. This is motivated by Iurato's anatomical studies of the rat cochlea, in which he observed that the main supporting bundles of the spiral lamina continue directly into the fibers of the basilar membrane (Iurato, 1962), suggesting a clamped end condition. The fibers on the other side of the Basilar Membrane (BM) continue directly into the spiral ligament but suddenly become thinner prior to joining the spiral ligament, which suggests a simply supported boundary condition. However, the movements at the boundaries of the BM are difficult to observe, thus leaving open the possibility for other boundary conditions. For this reason, and perhaps for simplicity, other authors have chosen to use simply supported boundary conditions along both edges (Naidu and Mountain, 2007). In order to explore the effect of changing boundary conditions on the material properties, we have carried out computations using both sets of boundary conditions: (SS) simply supported at both ends and (CS) clamped at the spiral lamina but simply supported at the spiral ligament.

III. BEAM MODEL

The first step in our procedure is to make use of a beam model to produce an initial estimate of the local elastic modulus E_y. The width of the beam is taken to be the probe's diameter: 10 μm in Naidu and Mountain (1998), 25 μm in Emadi *et al.* (2004). This is the same as assuming that the cochlear partition is perfectly orthotropic.

Figure 2 is a schematic of the beam model under probe load (with CS boundary conditions).

The elastic modulus calculated from the beam model (Budynas, 1999) for CS boundary condition is

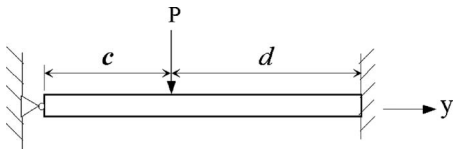

FIG. 2. Schematic of a beam model under load with one end simply supported and the other clamped.

$$E = \frac{-dc^2[3L(d^2 - L^2) + c(3L^2 - d^2)]}{12IL^3}k \tag{1}$$

and for SS boundary condition is

$$E = \frac{-dc(2c^2 - 2cL)}{6IL}k, \tag{2}$$

where k is the point stiffness of the beam, $L=c+d$ is the length of the beam, $I=wh^3/12$ is the area moment of inertia of the beam, w is the beam width, taken to be the probe diameter, and h is the beam thickness. Both the thickness and length of the beam, h and L, are taken from BM thickness and width as measured by Schweitzer *et al.* (1996). Note that these are dehydrated properties. These properties are used throughout this paper; we use Schweitzer *et al.*'s measurements because they also include information on fiber band thickness, which is important for our composite model, as explained in the following.

According to Naidu and Mountain (1998, Fig. 5 Panel D), the stiffness decreases along the longitudinal direction from base to apex as

$$k(x) = \frac{5.755}{e^{0.31x}}\frac{N}{m}. \tag{3}$$

According to Emadi *et al.* (2004, Fig. 3 Panel A) stiffness decreases as

$$k(x) = \frac{3.25}{e^{0.5x}}\frac{N}{m}. \tag{4}$$

For both equations, x has dimension millimeter.

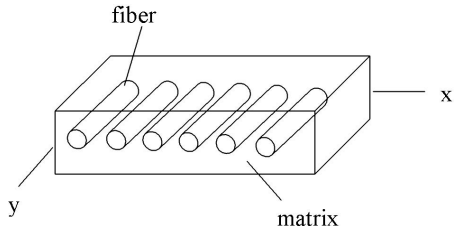

FIG. 3. Composite material with fibers and matrix.

TABLE I. Initial estimate of radial elastic modulus as determined from measured stiffness using a beam model.

Location from base (mm)	Beam length L (μm)	Thickness h (μm)	Position of applied load c (μm)	stiffness (N/m)	Boundary conditions	E_y (kPa)
1.14[a]	150	15.8	60	4.04	SS	79 700
					CS	40 600
3.99[a]	194	17.3	78	1.67	SS	54 300
					CS	27 700
6.612[a]	232	23.7	87	0.741	SS	15 300
					CS	8 060
7.3[a]	242	25.3	91	0.599	SS	11 500
					CS	6 080
7.3[b]	242	25.3	91	0.08	SS	601
					CS	317

[a]Naidu and Mountain (1998, 2001).
[b]Emadi *et al.* (2004).

Material properties were computed at three locations along the BM according to the experimental data from Naidu and Mountain (1998). These three locations are chosen because of the availability of experimental data for the dimensions of BM width and thickness for those locations in Schweitzer *et al.* (1996).

The first location is 1.14 mm from the base, the second is 3.99 mm from the base, and the last one is 6.612 mm from the base. An additional location 7.3 mm from the base is picked because it is the location at which the longitudinal coupling was measured by Emadi *et al.* (2004). Although the dimensions of the BM at this location are not given explicitly in Schweitzer *et al.* (1996), width and thickness of the BM can be estimated from Panels A and B in Fig. 5. Table I shows the stiffness and radial elastic modulus computed using this procedure at the different locations.

IV. PLATE MODEL

A. Composite material model

With an initial estimate of transverse elastic modulus in hand, we now move on to an orthotropic composite plate model. There are four independent material properties for the plate, but only two measurements at each location, requiring that additional assumptions be introduced. We use a composite plate model which allows us to reduce the number of unknowns. In particular, shear modulus, G_{xy}, and Poisson's ratio, ν_{xy} are estimated using the volume fraction method (Dowling, 1999).

TABLE II. Volume fractions at different locations taken from Schweitzer *et al.* (1996).

Location from base (mm)	1.14	3.99	6.612	7.3
V_r	0.192	0.089	0.05	0.041
V_m	0.808	0.911	0.95	0.959

In this method, the cochlear partition is treated as a fiber-reinforced composite. The fibers are considered as an isotropic linear elastic material with elastic constants E_r and υ_r, and the matrix another isotropic linear elastic material, with material properties E_m and υ_m. The composite has volume fractions occupied by the fibers and matrix, V_r, which is the ratio of fiber area to the total area and V_m, which is the ratio of matrix area to the total area, respectively. The composite plate model is shown in Fig. 3.

The relationships between the elastic moduli of the component materials and the effective elastic moduli of the composite plate are (Dowling, 1999)

$$E_x = \frac{E_r E_m}{V_r E_m + V_m E_r}$$

$$E_y = V_r E_r + V_m E_m \tag{5}$$

The lower and upper fiber band thicknesses can be estimated from Schweitzer *et al.* (1996), Panels B and C in Fig. 7. We make the simplifying assumption that the fiber bands are fully dense. The fibers are then treated as uniformly distributed throughout the thickness, maintaining these volume fractions. From the information from Schweitzer *et al.* (1996), the cross-sectional areas of the fibers and matrix are estimated, leading to the volume fractions V_r and V_m, listed in Table II.

We have an estimate of E_y based on the beam model, and have arbitrarily chosen E_x (recall for our procedure we chose an E_x,compute a space constant, and iterate to match experiment). We can therefore compute the required values of E_r and E_m as follows:

$$E_r = \frac{E_x V_r^2 - E_x V_m^2 + E_y}{2V_r} \pm \frac{\sqrt{E_x^2 V_r^4 - 2E_x^2 V_r^2 V_m^2 - 2E_x E_y V_r^2 + E_x^2 V_m^4 - 2E_x E_y V_m^2 + E_y^2}}{2V_r}, \tag{6}$$

$$E_m = \frac{-E_x V_r^2 + E_x V_m^2 + E_y}{2V_m} \mp \frac{\sqrt{E_x^2 V_r^4 - 2E_x^2 V_r^2 V_m^2 - 2E_x E_y V_r^2 + E_x^2 V_m^4 - 2E_x E_y V_m^2 + E_y^2}}{2V_m}. \tag{7}$$

The shear moduli of the component materials are then directly computed from (Dowling, 1999),

$$G_r = \frac{E_r}{2(1+\nu_r)},$$

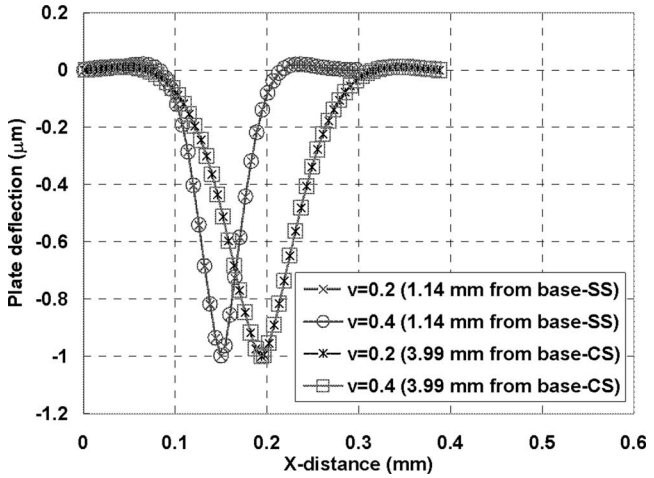

FIG. 4. Comparison of vertical displacement computed with different fiber Poisson's ratios for two different locations and boundary conditions. The Poisson ratio of the fiber has little impact on the result.

$$G_m = \frac{E_m}{2(1+\nu_m)}. \tag{8}$$

So we have the shear modulus of the composite (Dowling, 1999),

$$G_{xy} = \frac{G_r G_m}{V_r G_m + V_m G_r}. \tag{9}$$

We still need to compute the Poisson ratio of the composite plate. The Poisson's ratio of tissue ranges widely. Two different sets of Poisson's ratios ν_r=0.2 (Jurvelin *et al.*, 1997), which is estimated from bovine humeral articular cartilage, and ν_r=0.4 (Lai-Fook *et al.*, 1976), which is estimated from dog lung tissue, are investigated. Figure 4 shows that the choice of this parameter does not have a major impact on our results. The ground substance behaves as a layer of incompressible fluid (Miller, 1985), so we take ν_m=0.5. From these two component Poisson ratios and the volume fractions, we can compute the two Poisson ratios for the composite orthotropic plate (Dowling, 1999),

$$\nu_{yx} = V_r \nu_r + V_m \nu_m$$

$$\nu_{xy} = \frac{E_x}{E_y}\nu_{yx} \tag{10}$$

B. Analytic linear plate model

At this point, all four plate properties are defined. It is now possible to proceed to an orthotropic linear plate solution and compared computed and measured stiffness and space constant. The governing equation for a linear orthotropic Kirchhoff plate under a distributed load is Timoshenko, 1959

$$D_x \frac{\partial^4 w}{\partial^4 x} + 2D_{xy}\frac{\partial^4 w}{\partial^2 x \partial^2 y} + D_y \frac{\partial^4 w}{\partial^4 y} = q(x,y), \tag{11}$$

where

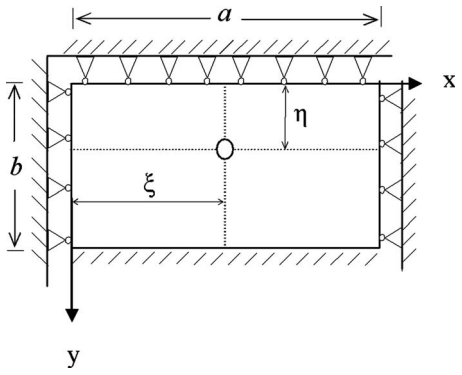

FIG. 5. Schematic of plate boundary conditions and load area.

$$D_x = \frac{E_x h^3}{12(1-\nu_{xy}\nu_{yx})} \tag{12}$$

is the flexural rigidity of the plate in x direction,

$$D_y = \frac{E_y h^3}{12(1-\nu_{xy}\nu_{yx})} \tag{13}$$

is the flexural rigidity of the plate in y direction,

$$D_{xy} = \frac{E_x h^3 \nu_{yx}}{12(1-\nu_{xy}\nu_{yx})} + \frac{G_{xy} h^3}{6} \tag{14}$$

is the tensional rigidity of the plate, and $q(x,y)$ is the normal load per unit area applied on the plate. The quantity h is the plate thickness, and E_x, E_y, G_{xy}, ν_{xy}, and ν_{yx} are the orthotropic plate material properties as described previously.

In the experiments, the load is applied on the middle of the pectinate zone. The load contact area is taken to be a circle whose diameter is the same as that of the probe. $q(x,y)$ is taken to be a uniform pressure over that contact area. Figure 5 is a schematic for one of the two choices of boundary conditions (CS).

The analytic displacement solutions for a circular region of distributed load with rectilinear boundary conditions have been derived based on plate theory (Szilard, 2004; Whitney, 1987; Ugural, 1999). The solution for the simply supported plate under circular load can be written as

$$w = \sum_{m=1}^{\infty}\sum_{n=1}^{\infty}\left[\frac{\dfrac{4P}{ab\pi^4}\displaystyle\int_0^{2\pi}\int_0^{c}\sin(\alpha)\sin(\beta)\rho\, d\rho\, d\theta}{D_x\dfrac{m^4}{a^4} + 2D_{xy}\dfrac{m^2 n^2}{a^2 b^2} + D_y\dfrac{n^4}{b^4}} \times \sin\left(\frac{m\pi x}{a}\right)\sin\left(\frac{n\pi y}{b}\right)\right], \tag{15}$$

where

$$\alpha = \left(\frac{m\pi(\xi+\rho\cos(\theta))}{a}\right),$$

$$\beta = \left(\frac{n\pi(\eta + \rho \sin(\theta))}{a} \right), \tag{16}$$

where a is the length of the plate, b is the width of the plate, c is the radius of the circle of load, P is the total load, ξ is the load location in the x direction, η is the load location in the y direction.

The solution for the one edge clamped and three edges simply supported with a circular load can be written as

$$w = \sum_{m=1}^{\infty} \sum_{n=1}^{\infty} \left[A \sin\left(\frac{m\pi\lambda_2 y}{a} \right) \cosh\left(\frac{m\pi\lambda_1 y}{a} \right) + B \cos\left(\frac{m\pi\lambda_2 y}{a} \right) \sinh\left(\frac{m\pi\lambda_1 y}{a} \right) + C \sin\left(\frac{n\pi y}{b} \right) \right] \sin\left(\frac{m\pi x}{b} \right), \tag{17}$$

where

$$C = \sum_{m=1}^{\infty} \sum_{n=1}^{\infty} \frac{\frac{4P}{ab\pi^4} \int_0^{2\pi} \int_0^c \sin(\alpha)\sin(\beta)\rho \, d\rho \, d\theta}{D_x \frac{m^4}{a^4} + 2D_{xy} \frac{m^2 n^2}{a^2 b^2} + D_y \frac{n^4}{b^4}}, \tag{18}$$

where α and β are defined in Eq. (16)

$$B = \frac{-Cna \cos(n\pi) \sin\left(\frac{m\pi\lambda_2 b}{a} \right) \cosh\left(\frac{m\pi\lambda_1 b}{a} \right)}{mb(-D + E - F)}, \tag{19}$$

where

$$D = -\lambda_2 \sinh\left(\frac{m\pi\lambda_1 b}{a} \right) \cosh\left(\frac{m\pi\lambda_1 b}{a} \right),$$

$$E = \lambda_1 \cos\left(\frac{m\pi\lambda_2 b}{a} \right) \sin\left(\frac{m\pi\lambda_2 b}{a} \right) \left[\cosh\left(\frac{m\pi\lambda_1 b}{a} \right) \right]^2,$$

$$F = \lambda_1 \sin\left(\frac{m\pi\lambda_2 b}{a} \right) \cos\left(\frac{m\pi\lambda_2 b}{a} \right) \left[\sinh\left(\frac{m\pi\lambda_1 b}{a} \right) \right]^2, \tag{20}$$

$$A = \frac{-C \sinh\left(\frac{m\pi\lambda_1 b}{a} \right) \cos\left(\frac{m\pi\lambda_2 b}{a} \right)}{\sin\left(\frac{m\pi\lambda_2 b}{a} \right) \cosh\left(\frac{m\pi\lambda_1 b}{a} \right)}, \tag{21}$$

and λ_1 and λ_2 are two constants

$$\lambda_1 = \mathrm{Re}\left\{ \sqrt{\frac{D_{xy} \pm \sqrt{D_{xy}^2 - D_x D_y}}{D_y}} \right\},$$

$$\lambda_2 = \mathrm{Im}\left\{ \sqrt{\frac{D_{xy} \pm \sqrt{D_{xy}^2 - D_x D_y}}{D_y}} \right\}. \tag{22}$$

Figure 6 shows the results for an analytic model after iteration of the values of E_y and E_x to produce a match to the point stiffness and space constant reported in Naidu and Mountain (1998, 2001) at $x=3.99$ mm from the base. Identical iterative procedures were applied at the other locations to produce the material properties shown in Table III. We emphasize again that these are based on a *linear* composite analytic plate model. Note that the linear plate only deflects normal to its surface. Thus, in matching the space constant, it is necessary to use the assumption of Naidu and Mountain that the observed *lateral* deflections of the plate are proportional to *out of plane* deflections. It is to explore the validity of this assumption that we move on to the geometrically nonlinear plate model.

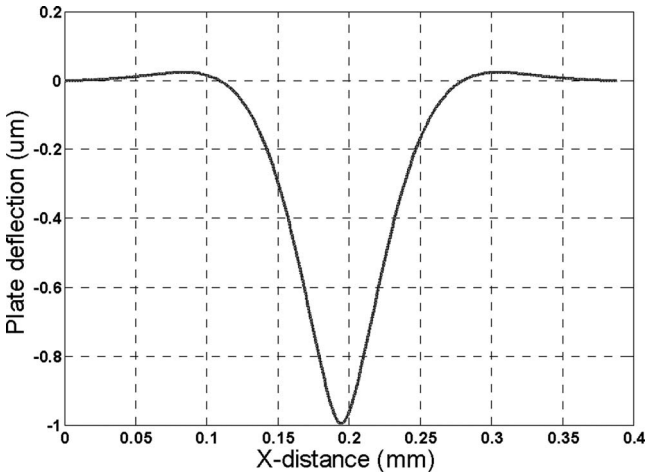

FIG. 6. Deflection profile using linear model.

C. Nonlinear finite element plate model

In Naidu and Mountain (1998, Fig. 2) the stiffness stays constant when the BM deflection remains in the 1–3 μm range. In addition, the displacements in this range (1–3 μm) are small compared to the plate thickness (16–25 μm). Thus, the use of a linear structural model for deflections of up to 3 μm appears to be justified. However, the space constant in Naidu and Mountain (2001) is based on the *lateral* displacement. A linear plate model gives no lateral displacements. On the other hand, a finite element analysis (FEA) solution using linear elastic material constitutive laws, but including *geometric nonlinearities*, will give nonzero lateral displacements. Such a solution was implemented in the finite element software package ABAQUS™.

Figure 7 shows the mesh that was used at location 1.14 mm from the base. The element used is S4R: a four-node doubly curved thin or thick shell element with reduced integration and hourglass control for finite membrane strains. A half-plate model is used as the plate model is symmetric about $x=0$. In order to reduce model size, the mesh is truncated in the x direction in a way that makes the symmetric model square. A rectangular plate model whose length is twice its width was also tested to verify that the truncation does not affect the model results. Convergence was tested by increasing the number of elements. A mesh with characteristic element length 0.6 μm is sufficient to produce a converged solution.

TABLE III. Material properties computed using the analytical linear model to match experimental point stiffness and space constant reported by Naidu and Mountain (1998, 2001). These results are based on the assumption of Naidu and Mountain, that the observed transverse displacements are linearly proportional to the out-of-plane displacements, an assumption we question in Sec. V.A.

							Composite plate properties determined by matching experiment			
Distance from base[a] (mm)	Space constant (μm)	b (μm)	η (μm)	Thickness (μm)	Stiffness (N/m)	Boundary conditions	E_x (kPa)	E_y (kPa)	G_{xy} (kPa)	ν_{xy}
1.14	13.2	150	60	15.8	4.042	SS	106	21500	35.5	0.0022
	13.2					CS	82.7	13100	27.6	0.0028
3.99	23.8	194	77.6	17.3	1.671	SS	150	8100	50.0	0.0088
	23.8					CS	148	4430	49.0	0.016
6.612	33.5	232	87	23.7	0.741	SS	36.0	1920	12.0	0.0091
	33.5					CS	42.0	1000	14.0	0.021
7.3	36.0	242	91	25.3	0.599	SS	26.0	1400	8.60	0.009
	36.0					CS	30.0	735	10.0	0.02

[a]Naidu and Mountain (1998, 2001).

V. DISCUSSIONS

A. Linearity versus nonlinearity

The geometrically nonlinear orthotropic plate model was first used to duplicate the previously conducted linear analytic analyses for both boundary conditions (using the material properties and geometry shown in Table III). A contour plot of the out-of-plane and lateral deflections computed with the nonlinear model are shown below in Fig. 9. An example of a comparison of the result with the analytical solution is shown in Fig. 8. The out-of-plane deflections are almost identical to the linear model results, verifying the FEA solution and demonstrating that the out-of-plane deflections are well captured by a linear model.

The lateral deflections, computed due to nonlinear geometric effects, are also shown. A cross section of the lateral deflection and out-of-plane deflection curves in the longitudinal direction through the centroid of the load region are shown in Fig. 10. The lateral deflections exhibit a different space constant than the out-of-plane deflections. It is the lateral deflection space constant that was measured by Naidu and Mountain.

The value of E_x and E_y in the geometrically nonlinear finite element model were iterated, starting from the linear results. The point stiffness and space constants reported by Naidu and Mountain were matched at each location along the BM. The space constant is now determined based on the *lateral* deflections. The shear modulus and Poisson ratio are determined using the volume fraction method described earlier. Table IV shows the parameters used and the resulting effective plate properties. Figure 11 shows how the results of material properties in Table IV vary along the longitudinal direction. The flexural rigidities of the plate are calculated using effective plate properties and presented in Table VI.

B. Comparison with hemicochlea experiment

In Emadi *et al.* (2004), the plateau stiffness at increasing distances from the upper middle turn (7.3 mm from the base)

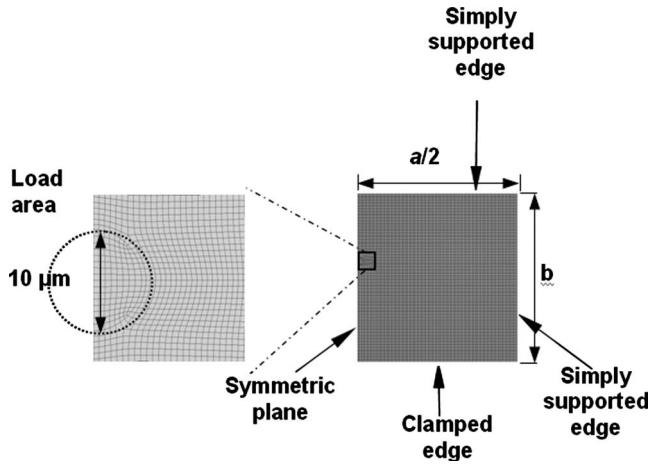

FIG. 7. One particular case (at a position of 1.14 mm from the base) of a meshed symmetric plate model in ABAQUS. 62 158 elements are used for this model, and the model is truncated to produce a square model.

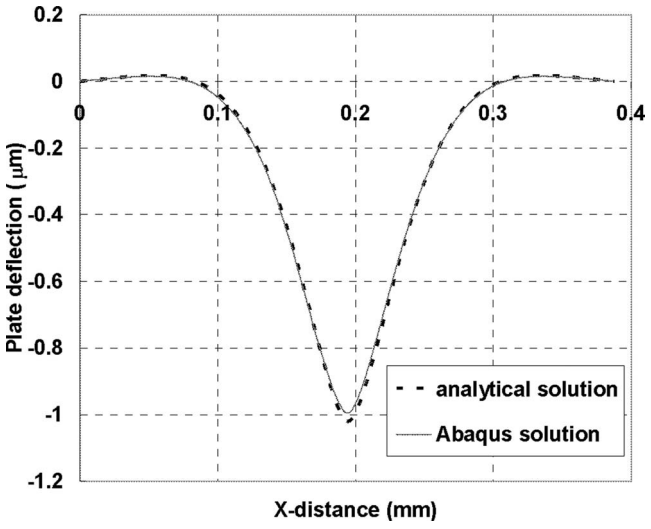

FIG. 8. Comparison of analytical solution with ABAQUS solution for SS boundary conditions at a position 3.99 mm from the base of the BM.

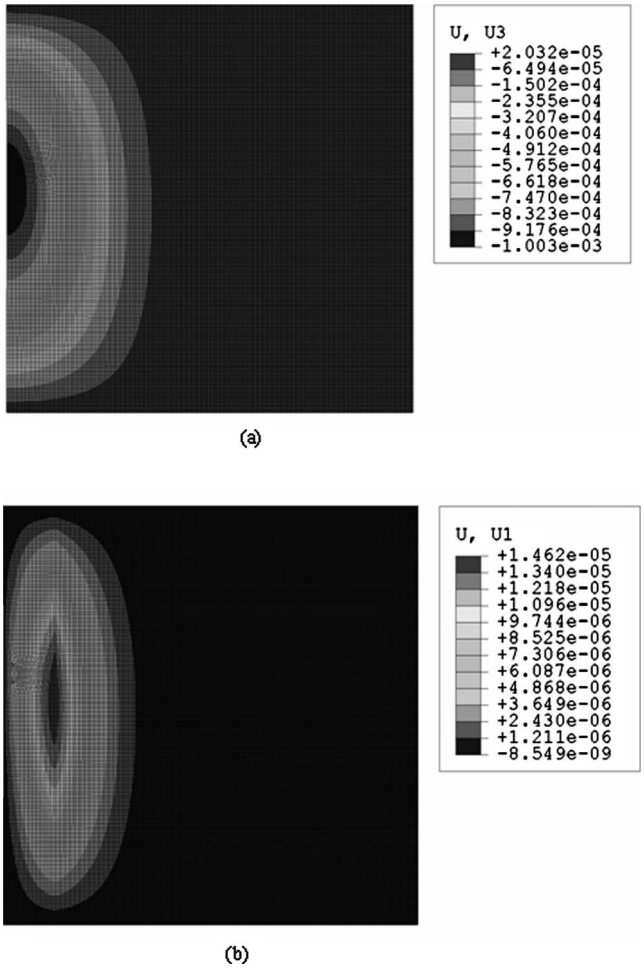

FIG. 9. Contour plot shows plate deflection at 1.14 mm from base. This is for an applied load of 4 μN distributed uniformly over the 5 μm radius contact region. (a) Out-of-plane deflection (mm) and (b) in-plane deflection (mm).

cut edge of a hemicochlea are measured. They used the change of stiffness very close to the cut edge to quantify the longitudinal coupling within the basilar membrane. They computed the space constant by fitting the plateau stiffness

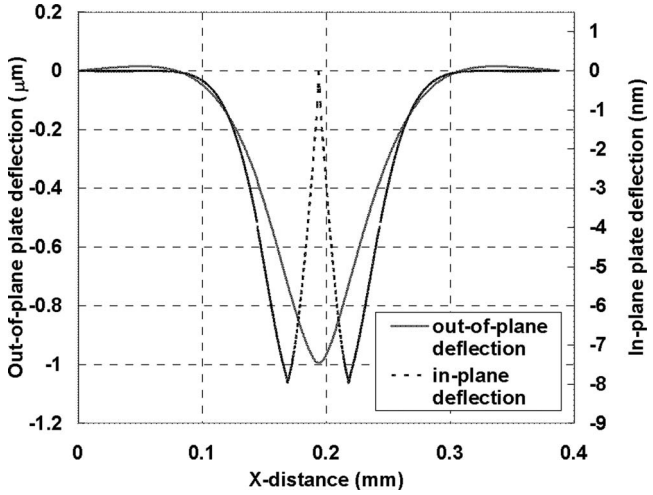

FIG. 10. Comparison of out-of-plane deflection and in-plane deflection for SS boundary conditions at a position 3.99 mm from the base of the BM. Out-of-plane deflection uses left vertical axis and in-plane deflection uses right vertical axis. Note that the space constant for the out-of-plane deflection and in-plane deflection are different.

with an exponential rise to an asymptote. The space constant they computed is 21 μm, which is smaller than a 40 μm space constant reported by Naidu and Mountain (2001), who pushed on the basilar membrane with a rigid probe and optically measured deflections of nearby structures. Thus, they stated there is relatively little longitudinal coupling within the pectinate zone of the basilar membrane in contrast to the intermediate levels of longitudinal coupling measured by Naidu and Mountain (2001).

As Emadi *et al.* and Naidu and Mountain used different methods to measure the space constant, and, indeed, different definitions for what the space constant is, it is difficult to compare their interpretation. We employ our orthotropic finite element plate model with a cut (free) edge to obtain the plateau stiffness profile in Emadi, *et al.* [2004, in Fig. 4(B)]. From this, we extract material properties from Emadi *et al.*'s experimental data. Figure 12 shows the stiffness profiles from Emadi *et al.*'s hemicochlea experiment and ABAQUS

TABLE IV. Results for material properties to match stiffness and *lateral* space constant. These are computed using the geometrically nonlinear orthotropic plate FEA model.

								Composite plate properties determined by matching experiment			
Distance from base[a] (mm)	Space constant (μm)	b (μm)	η (μm)	Thickness (μm)	Applied pressure load (kPa)	Stiffness (N/m)	Boundary conditions	E_x (kPa)	E_y (kPa)	G_{xy} (kPa)	ν_{xy}
1.14	13.2	150	60	15.8	51.5	4.042	SS	236	15300	78.6	0.0068
							CS	415	6640	138	0.028
3.99	23.8	194	77.6	17.3	21.27	1.671	SS	260	6240	86.7	0.020
							CS	326	2930	109	0.053
6.612	33.5	232	87	23.7	9.436	0.741	SS	76	1360	25.2	0.027
							CS	88.5	664	30.0	0.065
7.3	36.0	242	91	25.3	7.623	0.599	SS	47.7	1050	16.0	0.022
							CS	55.2	525	18.4	0.051

[a]Naidu and Mountain (1998, 2001).

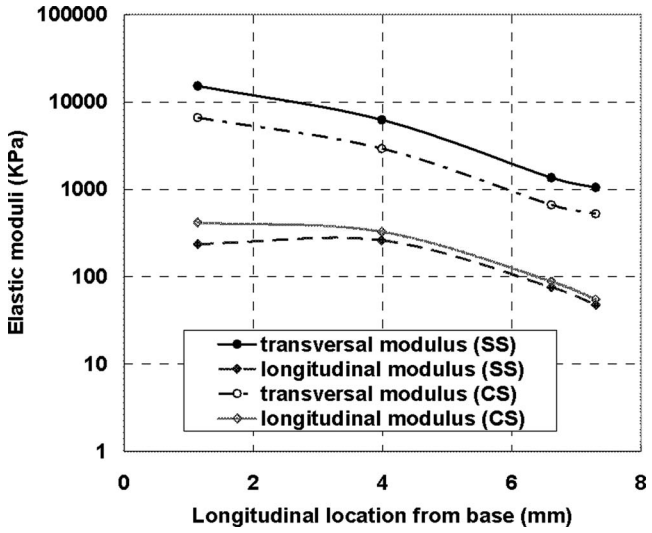

FIG. 11. Material property variations along the longitudinal direction for SS boundary condition.

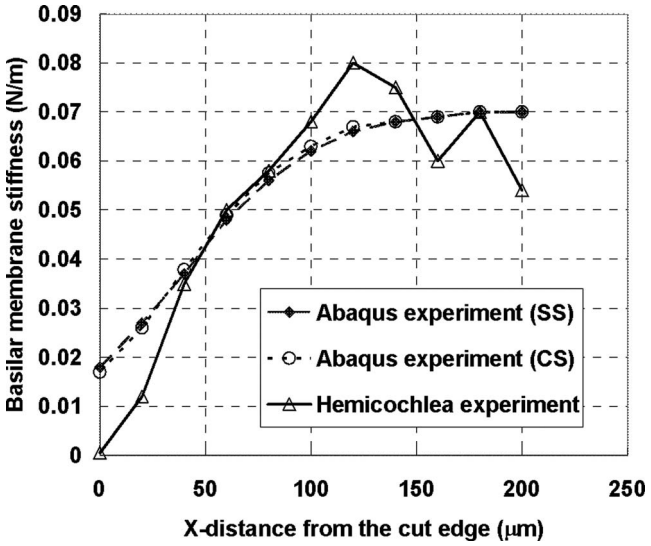

FIG. 12. Comparison of stiffness profile in hemicochlea experiment and ABAQUS experiments for different boundary conditions.

simulations for both types of boundary conditions. Stiffness measured by Emadi *et al.* at the cut edge is approximately an order of magnitude below the noise floor and so is treated in their work as effectively as zero. However, from a mechanics point of view, the stiffness at the edge cannot be truly zero; thus the model results, which include no noise, will always show a nonzero stiffness at the edge. The asymptotic stiffness is 0.07 N/m in Emadi *et al.* (2004), which we match. The variation of stiffness with distance from the cut edge is matched as closely as possible, giving a stiffness that gradually increases at distance increments up to the asymptotic stiffness, as shown in Fig. 12.

Attempts had been made to use ABAQUS data to fit the hemicochlea data for the points close to the cut edge before we came to the final fit curve. When the cut edge and the measured point closest to the cut edge are matched well with the hemicochlea data, the stiffness reduces and does not reach the stiffness far from the edge. We believe it is important to match the stiffness far from the edge. The discrepancy close to the cut edge can be explained by the possibility that the edge was damaged, whereas the cochlea was cut in half. In addition, the probe is 25 μm in diameter, which is relative large compared to the distance from the edge for the closest point. As the cut edge cannot support much force, it is also possible that the probe might slip.

The material properties determined to produce this matched result for the hemicochlea experiment are shown in Table V. Using these material properties, we are then able to compute a Naidu and Mountain space constant from Emadi *et al.*'s experimental data. This space constant is 185 μm for SS boundary conditions and 126 μm for CS boundary conditions. These space constants demonstrate considerable longitudinal coupling is present in Emadi *et al.*'s results. Indeed, their results seem to suggest a greater degree of coupling than is present in the data of Naidu and Mountain, where the space constant at this location was 36 μm.

TABLE V. Material properties obtained to match hemicochlea stiffness experiment.[a]

Boundary condition	E_x (kPa)	E_y (kPa)	G_{xy} (kPa)	ν_{xy}
SS	26	48	8.69	0.2645
CS	23	25	7.7	0.4436

[a]Emadi *et al.* (2004).

C. Probe area

In an experiment the contact area of the probe with the BM may not be precisely known. The maximum contact area is the total size of the probe, a 5 μm radius for the experiments of Naidu and Mountain, a 12.5 μm radius for Emadi *et al.* In order to investigate the sensitivity of the results to probe contact area, four different load areas, with radii 2, 5, 8, and 12.5 μm were investigated in both analytical and finite element solutions. In all cases, the results indicate that the probes with radius from 2 to 12.5 μm have little effect on the shape of the deflected region. An example result is shown below in Fig. 13.

Gueta *et al.* (2006) indicated that two different research groups obtained similar indentation shape on the tectorial membrane when both used nanoscale indenters but there was no agreement between the results when microscale indenters were used. They used a microscale indenter with radius 1 μm, whereas the other group used 5 μm. The 5 μm radius indenter is about half of the width of the tectorial membrane, which caused significant difference from the results measured by a 1 μm radius indenter, which is only 1/10 of the width of the tectorial membrane. The basilar membrane is much wider, 150–250 μm wide, and does not show much variation in our computations for radii of 2–12.5 μm. We suggest that the probe size has little effect on the deflection shape when it is small compared with the dimensions of the object being measured, but still larger than the embedded fibers.

TABLE VI. Composite plate flexural rigidity computed using plate material properties.

Distance from base (mm)	b (μm)	Thickness (μm)	Boundary conditions	Composite plate flexural rigidity computed using plate material properties D_x (N m)	D_y (N m)	D_{xy} (N m)
1.14[a] (Naidu & Mountain)	150	15.8	SS	7.78×10^{-11}	5.044×10^{-9}	8.597×10^{-11}
			CS	1.38×10^{-10}	2.21×10^{-9}	1.526×10^{-10}
3.99[a] (Naidu & Mountain)	194	17.3	SS	1.133×10^{-10}	2.72×10^{-9}	1.29×10^{-10}
			CS	1.443×10^{-10}	1.297×10^{-9}	1.628×10^{-10}
6.612[a] (Naidu & Mountain)	232	23.7	SS	8.54×10^{-11}	1.53×10^{-9}	9.72×10^{-11}
			CS	1.014×10^{-10}	7.61×10^{-10}	1.16×10^{-10}
7.3[a] (Naidu & Mountain)	242	25.3	SS	6.51×10^{-11}	1.43×10^{-9}	7.47×10^{-11}
			CS	7.64×10^{-11}	7.265×10^{-10}	8.67×10^{-11}
7.3[b] (Emadi *et al.*)	242	25.3	SS	4.03×10^{-11}	7.44×10^{-11}	4.313×10^{-11}
			CS	3.95×10^{-11}	4.29×10^{-11}	3.98×10^{-11}

[a]Naidu and Mountain (1998, 2001).
[b]Emadi *et al.* (2004).

D. Stiffness linearity

In Fig. 2 in Naidu and Mountain (1998), the stiffness measured in the 1–3 μm deflection range is approximately constant. That is to say, the deflection versus applied force curve is linear. The stiffness linearity of the geometrically nonlinear FEA plate model was examined by applying double and triple the test load. Figure 14 below shows the FEA results for center point deflection for both boundary conditions. The geometric nonlinearity contributes approximately 10% nonlinear stiffening at a displacement of 3 μm. This appears to be within the experimental error seen in Naidu and Mountain (1998, Fig. 2).

E. Basilar membrane dimensions

The basilar membrane dimensions used in the models were reported by Schweitzer *et al.* (1996), which were derived from fixed tissue. The fixation process results in a decrease in the thickness of the basilar membrane. The reason we used the dimension data of Schweitzer *et al.* for the basilar membrane is that they also reported the fiber band dimensions, which are essential for the volume fraction method. In addition, the basilar membrane does not have a uniform thickness along radial direction, but the curvature of the membrane is not known. To simplify the problem, we used a uniform thickness and a flat plate. The maximum thickness value for a given longitudinal position in Schweitzer *et al.* is used as the uniform thickness of our plate. When applying the material properties calculated in this paper to model the BM as a plate, the reader should use the same thickness that we use for the computations. Alternatively, the reader can use the plate properties from Table VI.

VI. CONCLUSION

The effective material properties of the gerbil BM were determined from experimental data using a geometric nonlinear orthotropic plate model implement using a finite ele-

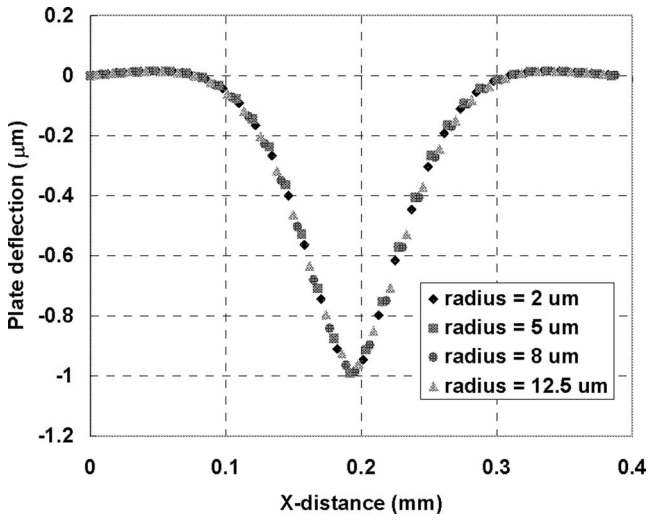

FIG. 13. Comparison of contact area effect for ABAQUS solution.

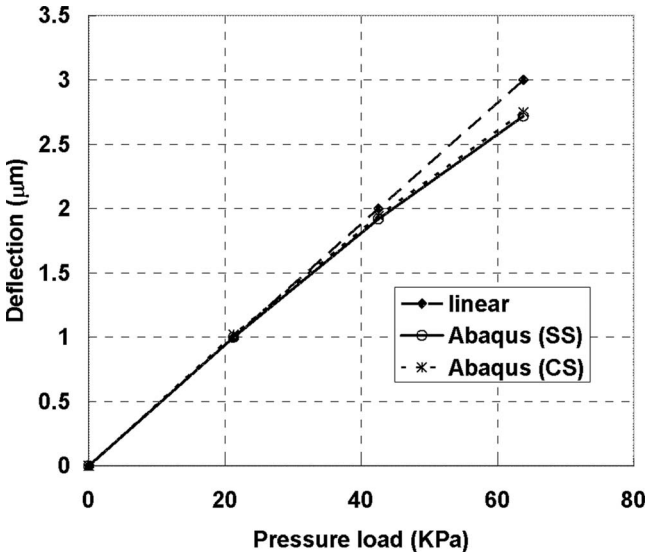

FIG. 14. Plate model linearity in the constant stiffness range at 3.99 mm from base.

ment framework. It is important to recognize that an orthotropic plate model cannot capture the full complexity of the cochlea physiology. However, using a simple model reduces the number of free parameters, allowing them to be determined from available data. It is important that the reader understands that material properties are effective properties, which should be used only for a flat orthotropic plate of the same uniform thickness used to derive the properties. Alternatively, models can use the plate properties shown in Table VI.

The resulting model is useful as an effective plate, representing a combination of effects coming from the complex physiology. Some examples of the complexities that are subsumed into the plate model include: the effect of organ of Corti (Naidu and Mountain, 1998; 2001), the effect of tectorial membrane (Emadi *et al.*, 2004), and the effect of radial variations. A variety of computations were conducted to explore different possibilities related to *in vivo* experiments as detailed in the following.

Different probe sizes were investigated in the simulations and it was shown that the exact contact area between probe and BM does not affect the results for probes of radius 2–12.5 μm. Under the same total load, by choosing a contact area radius of 2–12.5 μm, the plate deformed similarly.

The space constant for the out-of-plane deflection, computed by both linear and geometrically nonlinear models, is very different than the space constant for in-plane deflections. Computation of the in-plane deflection requires a geometrically nonlinear model. The results from the geometric nonlinear model demonstrate that such a model is necessary to interpret the experimental data of Naidu and Mountain, and thus produce an improved estimate of material properties for the BM. The assumption that *lateral* deflection is proportional to *vertical* deflection is inaccurate, and a purely linear model will produce imprecise estimates of material properties even for small deflections.

Using the point stiffness and space constant data from Naidu and Mountain (1998, 2001) and Emadi *et al.* (2004), a complete set of orthotropic plate properties was determined using a geometrically nonlinear model and two possible boundary conditions. For both simple supported (SS) and clamped-simply supported (CS) boundary conditions, a decrease of radial modulus is observed from base to apex. For SS (CS) boundary conditions, the radial modulus varies from 15 MPa (6.6 MPa) to 1 MPa (0.5 MPa) from the base to the upper middle turn of gerbil cochlea; in the same region the longitudinal modulus decreases from 0.2 MPa (0.4 MPa) to 0.05 MPa (0.05 MPa). From these results, it can be seen that the orthotropy varies along the length of the cochlear partition from a maximum of 65 close to the base to a minimum of 10 in the upper middle turn. This can be explained by the longitudinal decrease in thickness of fiber bands (Schweitzer *et al.*, 1996), which mainly contribute to the material properties in the transverse direction. For SS boundary conditions, both moduli are larger than for CS boundary conditions, as expected. The orthotropy ratio is similar for either choice of boundary conditions.

Naidu and Mountain observed that the BM of the gerbil is nearly isotropic at the apex and calculated an orthotropy ratio of 2 at the apex (Naidu and Mountain, 2007). Our orthotropy ratio is about 20 for SS boundary conditions and 10 for CS conditions at the upper middle turn (two thirds of the distance to the apex), which is a similar result. Skrodzka used a longitudinal elastic modulus 200 kPa and a transverse elastic modulus 250 kPa for human basilar membrane (Skrodzka, 2005), indicating a constant orthotropic ratio of 2.5 along the basilar membrane, which is close to our orthotropy ratio toward the apex. Gross properties of chinchilla basilar membrane used in a three-dimensional nonlinear active cochlear model by Lim and Steele were taken as 1.0 GPa for transverse modulus and 0.01 GPa for longitudinal modulus along the entire length of the BM (Lim and Steele, 2002). This 100 orthotropy ratio is close to our orthotropy ratio at the base of gerbil cochlea.

The different methods for measuring space constant by Emadi *et al.* and Naidu and Mountain were reconciled through the plate model presented in this paper. Material properties were retrieved through matching a stiffness profile in Emadi *et al.* (2004) and then used in the same model as that of Naidu and Mountain. The material properties determined from the experiment of Emadi *et al.* were used to simulate a Naidu and Mountain space constant. For the experimental data of Emadi *et al.*, this resulted in a space constant of 185 μm for SS boundary conditions, and 126 μm for CS boundary conditions. Both of these results are considerably higher than the 36 μm space constant measured by Naidu and Mountain at this location, demonstrating that the data of Emadi *et al.* also shows considerably longitudinal coupling.

Stiffness measured by Naidu and Mountain differ significantly from that by Emadi *et al.* The material properties estimated using these two sets of data thus also differ. The major difference is in the radial elastic modulus. This suggests something fundamentally different between the different experimental setups used by these two research group. Naidu and Mountain used isolated turn preparation for the cochlea experiments, in which the turn of interest was isolated while the adjacent turns were removed. The resulting preparation consisted of an entire cochlea turn with the OC and its attachments to the spiral lamina and spiral ligament intact. Emadi *et al.* cut the cochlea from apex to base along the modiolar plane. The cut effectively removed one half of the cochlea and left behind a hemicochlea. We suggest that these differences in preparation may be the cause of the different observed material properties. As stated earlier, the difference is not caused by the different probe sizes used by the two groups. Both experimental data sets do show considerable longitudinal coupling, but they do not result in identical material properties as derived by the methods of this paper.

These results all indicate that longitudinal coupling in the gerbil BM is significant, with orthotropy ratios on the order of 1–100, increasing from apex to base. Dynamic models of traveling wave motion in the passive cochlea demonstrate that low orthotropy ratios result in a more spatially distributed BM response, which would lead to less frequency discrimination. The next step in this work is to implement a

dynamic model using these material properties. The details of how this will affect the modeled dynamic response remain to be seen.

Allaire, P., Raynor, S., and Billone, M. (**1974**). "Cochlear partition stiffness-composite beam model," J. Acoust. Soc. Am. **55**, 1252–1258.

Budynas, R. G. (**1999**). *Advanced Strength and Applied Stress Analysis* (McGraw-Hill, New York).

Dowling, N. E. (**1999**). *Mechanical Behavior of Materials* (Prentice-Hall, Englewood Cliffs, NJ).

Edge, R. M., Evans, B. N., Pearce, M., Richter, C. P., Hu, X., and Dallos, P., (**1998**). "Morphology of the unfixed cochlea," Hear. Res. **124**, 1–16.

Emadi, G., Richter, C. P. Dallos, and P. (**2004**). "Stiffness of the gerbil basilar membrane: Radial and longitudinal variations," J. Neurophysiol. **91**, 474–488.

Gueta, R., Barlam, D. Shneck, R. Z., and Rousso, I. (**2006**). "Measurement of the mechanical properties of isolated tectorial membrane using atomic force microscopy," Proc. Natl. Acad. Sci. U.S.A. **103**, 14790–14795.

Gummer, A. W., Johnstone, B. M., and Arstrong, N. J. (**1981**). "Direct measurement of basilar-membrane stiffness in the guinea-pig," J. Acoust. Soc. Am. **70**, 1298–1309.

Iurato, S. (**1962**). "Functional implications of the nature and submicroscopic structure of the tectorial and basilar membranes," J. Acoust. Soc. Am. **34**, 1386–1395.

Jurvelin, J. S., Buschmann, M. D., and Hunziker, E. B. (**1997**). "Optical and mechanical determination of Poisson's ratio of adult bovine humeral articular cartilage," J. Biomech. **30**, 235–241.

Lai-Fook, S. J., Wilson, T. A., Hyatt, R. E., and Rodarte, J. R. (**1976**). "Elastic constants of inflated lobes of dog lungs," J. Appl. Physiol. **40**, 508–513.

Lim, K. M., and Steele, C. R. (**2002**). "A three-dimensional nonlinear active cochlear model analyzed by the WKB-numeric method." Hear. Res. **170**, 190–205.

Lynch, T. J., Nedzelnitsky, V., and Peake, W. T. (**1982**). "Input impedance of the cochlea in cat," J. Acoust. Soc. Am. **72**, 108–130.

Miller, C. E. (**1985**). "Structural implications of basilar-membrane compliance measurements," J. Acoust. Soc. Am. **77**, 1465–1474.

Naidu, R. C., and Mountain, D. C. (**1998**). "Measurements of the stiffness map challenge a basic tenet of cochlear theories," Hear. Res. **124**, 124–131.

Naidu, R. C., and Mountain, D. C. (**2001**). "Longitudinal coupling in the basilar membrane," J. Assoc. Res. Otolaryngol. **2**, 257–267.

Naidu, R. C., and Mountain, D. C. (**2007**). "Basilar membrane tension calculations for the gerbil cochlea," J. Acoust. Soc. Am. **121**, 994–1002.

Neely, S. T., and Kim, D. O. (**1986**). "A model for active elements in cochlear biomechanics," J. Acoust. Soc. Am. **79**, 1472–1480.

Olson, E. S., and Mountain, D. C. (**1991**). "In vivo measurement of basilar membrane stiffness." J. Acoust. Soc. Am. **89**, 1262–1275.

Ramamoorthy, S., Deo, N. V., and Grosh, K. (**2007**). "A mechano-electro-acoustical model for the cochlea: Response to acoustic stimuli," J. Acoust. Soc. Am. **121**, 2758–2773.

Richter, C. P., Evans, B. N., Edge, R., and Dallos, P.(**1998**). "Basilar membrane vibration in the gerbil hemicochlea," J. Neurophysiol. **79**, 2255–2264.

Schweitzer, L., Lutz, C., Hobbs, M., and Weaver, S. (**1996**). "Anatomical correlates of the passive properties underlying the developmental shift in the frequency map of the mammalian cochlea," Hear. Res. **97**, 84–94.

Skrodzka, E. B. (**2005**). "Mechanical passive and active models of the human basilar membrane," Appl. Acoust. **66**, 1321–1338.

Steele, C. R., and Taber, L. A. (**1979**). "Comparison of WKB calculations and experimental results for 3-dimensional cochlear models," J. Acoust. Soc. Am. **65**, 1007–1018.

Szilard, R. (**2004**). *Theories and Applications of Plate Analysis* (Wiley, New York)

Timoshenko, S., and Woinowsky-Krieger, S. (**1959**). *Theory of Plates and Shells* (McGraw-Hill, NY).

Ugural, A. C. (**1999**). *Stress in Plates and Shells* (McGraw-Hill, New York)

Voldrich, L. (**1978**). "Mechanical-properties of basilar-membrane," Acta Oto-Laryngol. **86**, 331–335.

Whitney, J. M. (**1987**). *Structural Analysis of Laminated Anisotropic Plates* (Technomic Publ. Co., Inc., Lancaster, PA).